

See discussions, stats, and author profiles for this publication at: <https://www.researchgate.net/publication/51908239>

Molecular View of the Role of Fusion Peptides in Promoting Positive Membrane Curvature

ARTICLE *in* JOURNAL OF THE AMERICAN CHEMICAL SOCIETY · DECEMBER 2011

Impact Factor: 12.11 · DOI: 10.1021/ja207290b · Source: PubMed

CITATIONS

31

READS

32

2 AUTHORS, INCLUDING:



Siewert J Marrink

University of Groningen

206 PUBLICATIONS 13,919 CITATIONS

[SEE PROFILE](#)

Molecular View of the Role of Fusion Peptides in Promoting Positive Membrane Curvature

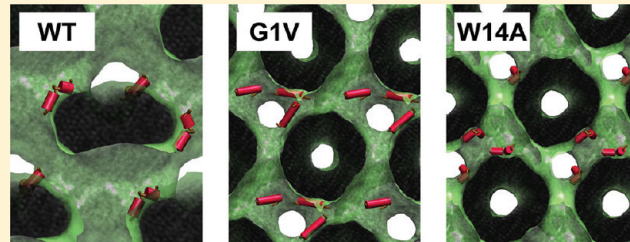
Marc Fuhrmans^{†,‡} and Siewert J. Marrink^{*,†}

[†]Groningen Biomolecular Sciences and Biotechnology Institute & Zernike Institute for Advanced Materials, University of Groningen, Groningen, The Netherlands

[‡]Universität Göttingen, Göttingen, Germany

Supporting Information

ABSTRACT: Fusion peptides are moderately hydrophobic segments of viral and nonviral membrane fusion proteins that enable these proteins to fuse two closely apposed biological membranes. In vitro assays furthermore show that even isolated fusion peptides alone can support membrane fusion in model systems. In addition, the fusion peptides have a distinct effect on the phase diagram of lipid mixtures. Here, we present molecular dynamics simulations investigating the effect of a particular fusion peptide, the influenza hemagglutinin fusion peptide and some of its mutants, on the lipid phase diagram. We detect a systematic shift toward phases with more positive mean curvature in the presence of the peptides, as well as an occurrence of bicontinuous cubic phases, which indicates a stabilization of Gaussian curvature. The wild-type fusion peptide has a stronger effect on the phase behavior as compared to the mutants, which we relate to its boomerang shape. Our results point to a different role of fusion peptides than hitherto assumed, the stabilization of pores rather than stalks along the fusion pathway.



INTRODUCTION

The fusion of the influenza virus to its intended host-cell is mediated by the hemagglutinin (HA) trimer. In its mature state, each HA monomer consists of two subunits: HA1, which is mainly involved in receptor binding, and HA2, which is believed to be responsible for the fusion process. HA2 is anchored to the viral membrane with a helical transmembrane domain close to its C-terminus and possesses an N-terminal fusion peptide, which becomes exposed after a conformational change of the protein's ectodomain at low pH (for a recent review, see ref 1). In *in vivo* experiments, both the transmembrane domain² and the fusion peptide³ as well as the conformational change of the ecto-domain of HA⁴ are required to complete fusion. While the transmembrane domain appears to require only a fixed length to be active,² the fusion peptide requires a more specific structure,⁵ indicating a complex role beyond the mere establishment of a contact to the target membrane.

Studies focusing on the fusion peptides alone show that, *in vitro*, the presence of only the fusion peptides is sufficient to induce lysis or vesicle fusion under suitable conditions.⁶ The fusion peptides also have a distinct effect on the phase diagram of lipid mixtures, decreasing the temperature at which cubic phases are observed⁷ and altering the lamellar-to-inverted hexagonal phase transition temperature in a concentration-dependent manner.⁸

The structures of the 20 amino acids long HA fusion peptide,⁹ as well as of the full length 23 amino acid long peptide¹⁰ at the fusogenic pH of 5.0, are available from NMR measurements in micelles revealing a characteristic boomerang shape:

Two amphiphilic alpha helical arms are joined by a relatively rigid linker region so that the hydrophobic parts of the helices face toward the inside of the kink. The degree of kinking depends on the peptide length, with an angle of approximately 105° found for the 20 residue peptide,⁹ and a close to 180° hairpin structure for the full length peptide.¹⁰ The peptide partitions to the lipid/water interface as was confirmed by polarized ATR-FTIR measurements.⁶ Among the mutants of the HA fusion peptide, two point mutants are known that are nonfusogenic *in vivo* and mainly differ from the wild-type (WT) in the angle between the helical arms. One is helical over almost the whole length and therefore linear (G1V),¹¹ while in the other the kink is inverted with respect to the wild-type with a less rigid linker region (W14A).⁵

Because of the general difficulty to devise experiments that give direct information on the fusion peptides' mode of action, computer simulations modeling the effect of the peptide on a lipid environment could greatly complement the experimental data. In particular, molecular dynamics (MD) simulations have proven to be a powerful tool in the study of membrane–protein interactions.^{12–15} Pertaining to the action of fusion peptides, computational work published so far is limited to studies of the structure and location of the peptide at lamellar and micellar interfaces (see, e.g., refs 16–18), which is probably a reflection of the limitation of the accessible system size and time scale in atomistically detailed simulations. Here, we try to

Received: August 3, 2011



overcome these computational limitations by using the coarse-grained MARTINI model,^{19,20} which has been successfully used to simulate the phase behavior of lipids^{21–23} and lipid/peptide systems.^{24–26} Starting from randomized mixtures of lipids and peptides, we observe the self-assembly of a large variety of phases depending on lipid type, hydration, and temperature, further modulated by the presence of the influenza HA fusion peptide and the G1V and W14A mutants. Thus, we are able to predict not only the effect of the fusion peptide on the lipid phase diagram, but also characterize the localization of the peptide within these phases at a near-atomic level of detail. Our results point to a different role of fusion peptides than hitherto assumed, stabilization of membrane pores rather than stalks. This puts the mechanism of action of fusion peptides in line with other membrane active peptides such as antimicrobial and cell penetrating peptides and offers a new angle on the traditional pathway of membrane fusion.²⁷

RESULTS

To study the ability of the HA fusion peptide to modulate the lipid phase diagram, we focus on DOPE (dioleoylphosphatidylethanolamine) and DOPC (dioleoylphosphatidylcholine) lipids. These lipids were chosen as they display a broad range of phases, ranging from predominantly lamellar states for pure DOPC to inverted-hexagonal for pure DOPE, as well as the so-called rhombohedral phase (“stalk” phase) observed for mixed PC/PE systems at low hydration. The inverted phases and stalk phase are in general believed to have a resemblance to intermediate states of the fusion process and are therefore appropriate to study the potential effect of fusion peptides. To construct the phase diagram, we performed self-assembly simulations of systems composed of 256 lipids and four peptides, corresponding to a mole fraction of peptides of almost 2%. The ratio of PC/PE, hydration level, and temperature were systematically varied. At each state point, multiple simulations were performed starting from a randomized initial distribution of the components. Each simulation was run for an effective time of 12 μ s, which proved to be long enough for the system to adopt a stable phase. Next to the WT HA fusion peptide, we considered the nonfusogenic point mutants G1V and W14A as well as the WT mutant at nonfusogenic pH. The conformation of the fusion peptides in our simulations was optimized with respect to the experimental NMR structures^{5,9,11} at micellar interface for the 20 residue long wild-type and both mutants (Figure 1). Details about the simulations can be found in the Methods.

In the following, we will first briefly discuss the self-assembly pathway and identification of the phase diagram, and proceed with a description of the modulating effects of the wild-type HA fusion peptide at pH 5.0. This will be followed by the results for the G1V and W14A mutants and the wild-type at pH 7.4.

Spontaneous Aggregation Approach Yields Distinct Phases. In our simulations starting from randomized positions of the constituents, the hydrophobic and hydrophilic components quickly separated, typically forming a three-dimensional network of water channels interwoven with an equally complex network of elongated micelles. Within the first microsecond, the topology of these initial aggregates rapidly changed as pores and stalks vanished. The further this assembly proceeded, the slower the changes took place; after typically 3 μ s, only fluctuating deformations of the shape but no more topological changes were observed. The aggregates remained stable during the remainder of the simulation time, totaling 12 μ s. Snapshots of a sample aggregation are shown in Figure 2.

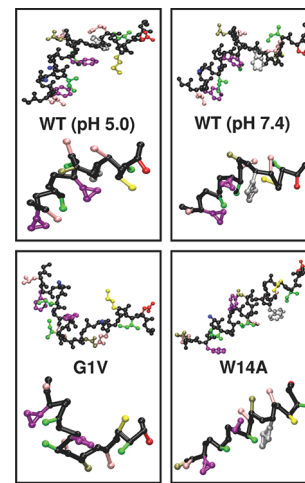


Figure 1. Structure of the HA fusion peptides considered in this work. Comparison of the representation of the fusion peptides in our coarse-grained model (bottom) with the NMR structures^{5,9,11} obtained at a micellar surface (top). The peptide backbone is shown in black and the side chains in colors, indicating the residue with pink for L and E, purple for F, blue for A, green for I, brown for N and V, gray for W, yellow for M, and red for D.

We assigned the adopted phase using the topology of the volume occupied by the hydrophilic headgroups and solvent as criterion, as described in the Methods. It should be noted that while we can be sure that the assembled phases possess a high degree of kinetic stability, they do not necessarily correspond to the state at thermodynamic equilibrium. Nevertheless, we observe a consistent and reproducible dependence of the assumed state on both the lipid composition and the presence of the different peptides throughout a large number of simulations. As such, we will interpret our results as representative of the true phase diagram of these systems. The phase diagram emerging from our simulation is shown in Figure 3 in the form of a bar plot. The phases adopted in the presence of the fusogenic wild-type peptide at pH 5.0 in lipid systems of either DOPE, DOPC, or their 1:1 mixture (as well as the corresponding peptide-free references) are shown, together with the effects on the phase diagram of the nonfusogenic W14A and G1V mutants and the WT at pH 7.4. Note that the simulations have been conducted over a range of temperatures (270–315 K) and hydration levels (8–12 waters per lipid), however, only a weak dependence on the exact state conditions was found in our simulations. For clarity, the data in Figure 3 are therefore collapsed across the entire temperature range and into three different levels of hydration (see legend). An indication of the temperature and hydration levels of the individual simulations can be found in the detailed phase diagram shown in the Supporting Information.

In the absence of peptides, the lipid phases observed in our simulations are consistent with the experimental phase diagram^{28,29} and with previous simulation results based on the same model.³⁰ The following two important trends are captured (cf., Figure 3): (i) upon increasing the amount of DOPE in the mixture, a shift from the lamellar to the inverted hexagonal phase as the predominant phase is observed, and (ii) at low hydration levels, the rhombohedral phase is stabilized. The rhombohedral phase, also denoted “stalk” phase, consists of a regular array of stalks connecting an otherwise lamellar system. Experimentally, the stalk phase was resolved by Yang and

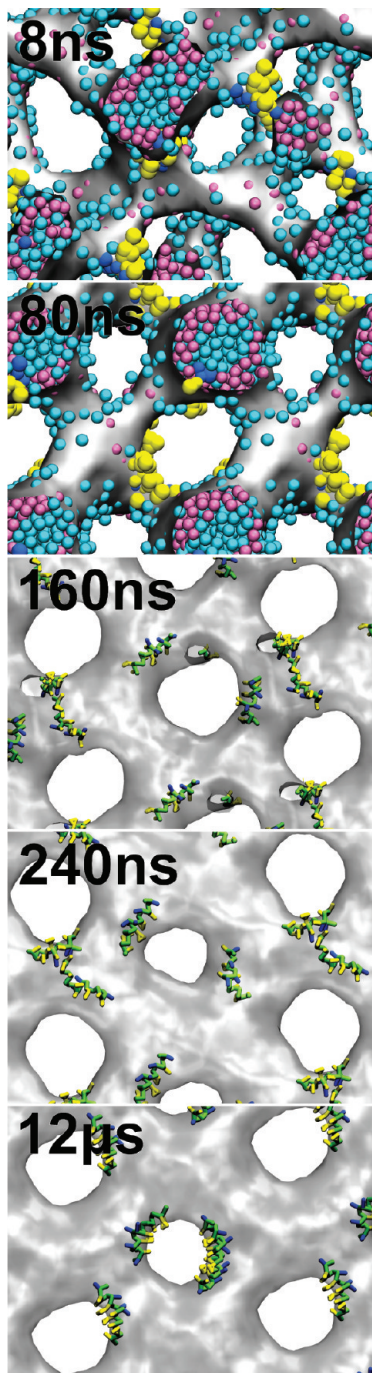


Figure 2. Snapshots illustrating a typical trajectory of a spontaneous aggregation. Shown is the assembly of DOPE into a stalk phase in the presence of the WT peptides (pH 5.0). Water molecules are shown in cyan, lipid headgroups in magenta, the peptides' backbones in green, and hydrophilic and hydrophobic side chains in blue and yellow, respectively. In addition, the lipid/water interface is shown as a gray surface. To better visualize the peptides' positions, we switch to a depiction showing only the interface and peptides as soon as the general shape of the stalk phase becomes apparent.

Huang,²⁹ and is observed predominantly for DOPC/DOPE mixtures in dehydrated samples, consistent with our simulated phase diagram.

HA Fusion Peptide Shifts Phase Diagram toward Rhombohedral and Lamellar Phases. When the WT fusion peptide in its fusogenic conformation is included, the phase

behavior changes significantly, with the largest change observed for pure DOPE (cf., Figure 3). The inverted hexagonal phase, which is exclusively observed for the peptide-free reference simulations except at the lowest hydration levels, is no longer found in the presence of the fusion peptides. Instead, stalk phases become the dominant phase. The stalk phases adopted by DOPE in the presence of the WT often show a resemblance to the inverted hexagonal phase, where the general shape of the cylindrical water channels is still visible, but the channels are connected by bridges of water and lipid headgroups (compare Figure 4A,B). At lower hydration, the DOPE/peptide system adopts stalk phases closer to the ideal rhombohedral geometry (Figure 4C).

In case of the 1:1 mixture of DOPE and DOPC, the systems containing no peptides adopt the stalk phase except at the highest hydration level simulated, where a lamellar phase is found for low temperatures. As compared to that, the simulations containing WT peptides are found to adopt the lamellar phase over a much broader range of temperature and hydration levels (Figure 4D). In those cases where stalk phases are still observed, they bear a much higher resemblance to the lamellar phase in comparison to the stalk phases observed with WT and pure DOPE; the density of stalks tends to be lower, and the curvature is often limited to the stalks and their neighborhood, with planar regions between (compare Figure 4E and C). The results for the simulations of pure DOPC show a trend similar to those for the 1:1 mixture with DOPE. While the peptide-free systems adopt the stalk phase at the lowest hydration level simulated, the simulations containing the wild-type peptides adopt the lamellar phase with not a single instance of the stalk phase even at the lowest hydration level (Figure 3).

Thus, the peptides appear to stabilize the stalk phase with respect to the inverted hexagonal phase, and the lamellar phase with respect to the stalk phase. No experimental observations of the stability of the rhombohedral stalk phase linked to fusion peptides are known to the authors. We predict that the WT fusion peptide has a significant effect; we expect stabilization of the stalk phase with PEs and destabilization with PCs.

HA Fusion Peptides Can Induce Inverted Cubic Phases.

Another apparent effect of the fusion peptides at pH 5.0 is the occurrence of bicontinuous cubic phases that are not observed in their absence (denoted by the cyan bars in Figure 3). Specifically, the single diamond phase²⁴ (Figure 4F) is observed in the presence of the wild-type peptide. The single diamond phase possesses a three-dimensional periodic interconnected network of hydrophilic groups that connects all aqueous components in a single continuous aggregate. In this aggregate, four water channels lined by lipid headgroups emerge from every junction in a tetrahedral manner. The same is true for the hydrophobic part of the system: all lipid tails are joined in a single continuous aggregate with a morphology identical to the one described for the hydrophilic groups. The phase can therefore be described as two mutually interpenetrating labyrinths of identical morphology, where a network of stalks defines a network of water channels and vice versa with the interface corresponding to the diamond triply periodic minimal surface.³¹ It has been predicted in a field theoretic study that pores and stalks in close proximity stabilize each other,³² presenting further evidence for the energetic feasibility of the single diamond phase. A detailed discussion of the single diamond phase, which to date is observed in silicio only, has been published separately.²⁴

Comparing our results in the presence of the peptides to experimental data, the stabilization of bicontinuous cubic phases

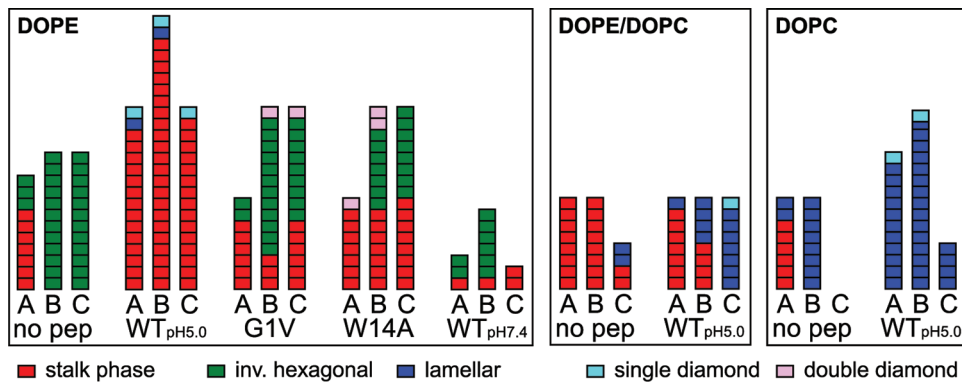


Figure 3. Bar plot showing the effect of the HA fusion peptide on lipid phase behavior. Overview of the phases adopted for pure DOPE, a 1:1 mixture of DOPE and DOPC, and pure DOPC. Results are shown for simulations containing either no peptides, or in the presence of the influenza HA fusion peptide (WT) both at fusogenic (pH 5.0) and at nonfusogenic pH (pH 7.4), and the nonfusogenic G1V and W14A mutants. A, B, and C indicate hydration levels of 8.0–8.9, 9.7–10.4, and 11.2–12.0 water molecules per lipid, respectively. Each block in the bar graph represents a single simulation, with the color indicating the phase adopted at the end of the simulation, after 12 μ s. The simulations have been conducted at temperatures between 270 and 315 K (see the Supporting Information for a detailed phase diagram).

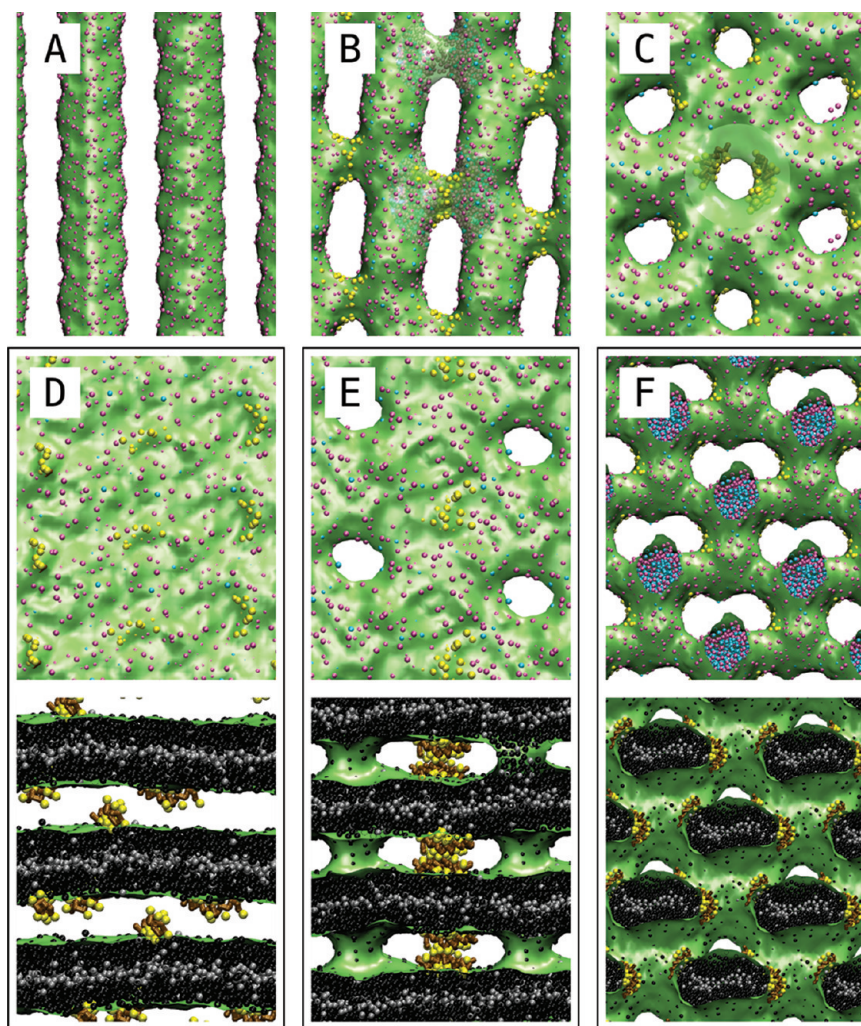


Figure 4. Images of lipid phases observed in the presence of the wild-type of the influenza HA fusion peptide. The snapshots, obtained at the end of the simulations, represent different morphologies: an inverted hexagonal phase adopted by pure DOPE in the absence of peptides (A), two stalk phases adopted by DOPE in the presence of the fusion peptide (B and C), a typical lamellar phase adopted by DOPC and the 1:1 mixture in the presence of the peptide (D), a typical stalk phase adopted by the 1:1 mixture in the presence of the peptide (E), and a single diamond phase adopted by DOPE, DOPC, and the 1:1 mixture in the presence of the peptide (F). For (D)–(F), two alternative views are given. Lipid tails are shown in gray for the distal ends and in black for the rest, glycerol moieties in magenta, water and headgroups in blue, and the backbone and side chains of the fusion peptide in brown and yellow, respectively. The surface separating the lipid tails from the rest of the system is shown in green. In some regions, the surface has been rendered transparent to reveal the underlying structure, omitting molecules blocking the view on the peptides when necessary.

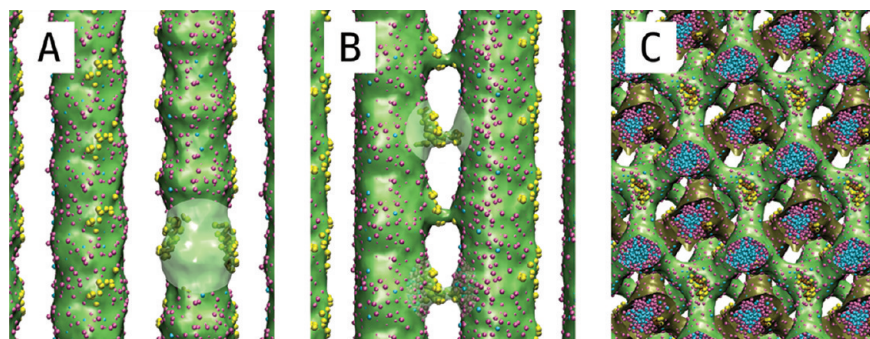


Figure 5. Images of lipid phases adopted by pure DOPE in the presence of nonfusogenic mutants of the influenza HA fusion peptide. The snapshots are of simulations with the G1V mutant, but are also representative for our simulations with the W14A mutant or the WT at pH 7.4. Shown are two inverted hexagonal phases (A and B), and a double diamond phase (C). The connections between the cylindrical water channels visible in (B) do not contain headgroups or solvent. The color representation is the same as in Figure 4. In some regions, the surface has been rendered transparent to reveal the underlying structure, omitting molecules blocking the view on the peptides when necessary.

in our simulations is in agreement with reports of a reduction of the temperature at which these phases form in vitro.^{7,8} Experimental findings of an induction of the inverted hexagonal phase⁷ at low peptide concentration, on the other hand, appear to disagree with our data. However, the experimental results are concentration dependent, and experiments using a higher peptide concentration comparable to the one used in our simulations in fact indicate a destabilization of the inverted hexagonal phase⁸ in agreement with our results.

Nonfusogenic Mutants and WT at Nonfusogenic pH Modulate Phase Diagram to a Lesser Extent. Simulations including the nonfusogenic G1V and W14A mutants in place of the WT peptide were performed for pure DOPE only. The results are shown in the form of bar graphs in Figure 3. A few snapshots are shown in Figure 5. The G1V and W14A mutants show a similar preference of the stalk over the inverted hexagonal phase as the wild-type, but at a reduced efficiency. In the presence of either mutant, the inverted hexagonal phase is still observed in approximately 50% of the simulations. Depending on the hydration level and temperature, the inverted hexagonal phase may look regular (i.e., well-separated water channels, Figure 5A), or closer to a stalk phase (Figure 5B). However, the topology of the lipid/water interface is identical in both cases, because the connections visible in Figure 5B only contain peptides but neither water nor headgroups. In contrast, the WT peptide establishes a proper porous connection (including water and headgroups) between the water channels in all simulations where a resemblance to the inverted hexagonal phase can be seen (compare Figures 4B and 5B). Apparently, the wild-type peptide is more efficient in stabilizing the stalk phase, at least in the pure PE system.

Like the WT, the mutant peptides are also observed to induce inverted cubic phases, indicated by the magenta bars in Figure 3. In contrast to the WT, however, the double diamond phase is formed rather than the single diamond phase. The double diamond phase is similar, with the defining difference that two isolated water compartments are formed, both of which have the same morphology as described for the single diamond phase. The hydrophobic components also form a periodic three-dimensional aggregate, a curved lipid bilayer separating the two aqueous labyrinths, with a midplane corresponding to the diamond triply periodic minimal surface. A snapshot of the double diamond phase formed in the presence of the G1V mutant is presented in Figure 5C.

To further validate our model and potentially distinguish effects due to amino-acid sequence from effects due to secondary structure, we also simulated a number of spontaneous aggregations including the WT peptide with a structure corresponding to NMR data at the nonfusogenic pH of 7.4.⁹ As shown in Figure 3, the results are similar to the findings for the nonfusogenic mutants. The stalk phase is found more often than in the peptide-free reference, but less often than in the simulations containing the WT with a structure corresponding to the fusogenic pH. Similar to the mutant peptides, the WT peptides at pH 7.4 are frequently found lying between the water channels of the inverted hexagonal phase without forming a porous connection.

In the simulations performed, no cubic phases were observed for the WT at pH 7.4. Because of the relatively small number of simulations performed, however, this finding may be due to insufficient statistics.

Molecular View of Peptide Embedding. To understand the ability of the peptides to modulate the lipid phase behavior, it is informative to consider the location of the peptides within the systems. The near-atomic resolution of the simulations allows us to pinpoint the exact positioning of the peptides in the different phases. Such information is hard to extract from experiment, and in particular for nonlamellar phases such information is currently lacking.

We first look at the embedding of the WT at the fusogenic pH 5.0 in a planar bilayer. For this, we use the simulations of DOPC, which lend themselves to straightforward comparison to published data. As illustrated in Figure 6, the peptides partition to the interface between the hydrophobic and the hydrophilic region where they sit with the hydrophobic side chains buried between the apolar groups corresponding to glycerol and the lipid tails, and the hydrophilic side chains facing the solvent. The N-terminal helix slightly penetrates into the hydrophobic core, while the C-terminal helix lies approximately parallel to the lipid water/interface, in good agreement with both experimental EPR data¹¹ and MD results using an atomistic representation.¹⁸

For the nonlamellar phases, experimental data are lacking. We find the general behavior to be similar to that of the lamellar phases. Both the wild-type and the mutant peptides partition to the lipid/water interface where they sit with the hydrophobic side chains penetrating slightly into the lipid tail region and the more polar side chains between the lipid headgroups. Figure 7 gives a comparison of the different peptides at nonlamellar

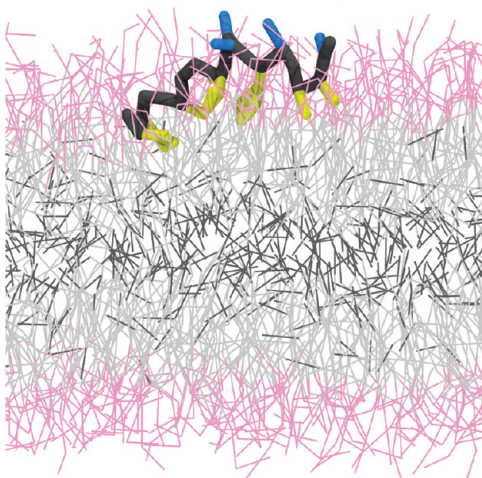


Figure 6. Positioning and embedding of the fusogenic WT peptide (pH 5.0) in a planar DOPC bilayer. The N-terminal helix slightly penetrates into the hydrophobic core, while the C-terminal helix lies approximately parallel to the lipid water/interface. Lipid headgroups are shown in magenta, and lipid tails are shown in gray (with black indicating the distal ends). The peptide's backbone is depicted in black, and hydrophilic and hydrophobic side chains are shown in blue and yellow, respectively. The peptide is shown with the N-terminus at the left and the C-terminus at the right.

interfaces. Specifically, we show the WT at pH 5.0 in the single diamond phase, and the G1V and W14A mutant in the double diamond phase. For all peptides, the general embedding is similar, and the peptides sit in a cradle-like lipid morphology. The sides of this lipid cradle are formed by glycerol moieties and headgroups replaced by the peptides' backbone, whereas

the bottom is formed by lipid tails that are oriented roughly parallel to the surface. Considering the global location of the peptides at the anisotropic lipid/water interface of the non-lamellar phases, the WT peptides show a strong tendency to colocalize with positive curvature components of the surface, as will be discussed in more detail in the Discussion.

In addition, Figure 7 shows the positioning of the WT peptide with a structure corresponding to the nonfusogenic pH of 7.4 in the stalk phase. Interestingly, the nonhelical, C-terminal arm of the peptide is embedded less deep than for the other peptides. Rather than being buried at the level of the glycerol moieties and having direct access to the lipid tail region, it is instead lodged between the hydrophilic headgroups, and the bottom of the cradle-like lipid configuration described above is composed of the glycerol backbone of the lipids. Using the stalk phase to compare the depth of embedding for the WT's structures at fusogenic and nonfusogenic pH, we find that the C-terminal arms were generally embedded less deep for the structure at pH 7.4 (data not shown).

■ DISCUSSION

Fusion Peptides Induce Positive Curvature Component Stabilizing Regions with High Gaussian Curvature. To rationalize our results, we use the concept of interface curvature, which has proven appropriate for the characterization and theoretical interpretation of lipid phases in general.³³ In this approach, the local shape of a surface is defined by its two principal curvatures, that is, the minimum and maximum geodesic curvature at a point, which determine the mean curvature as their average and the Gaussian curvature as their product. The mean curvature identifies the average bending deformation at a point (conventionally defined as positive for the surface of a micelle),

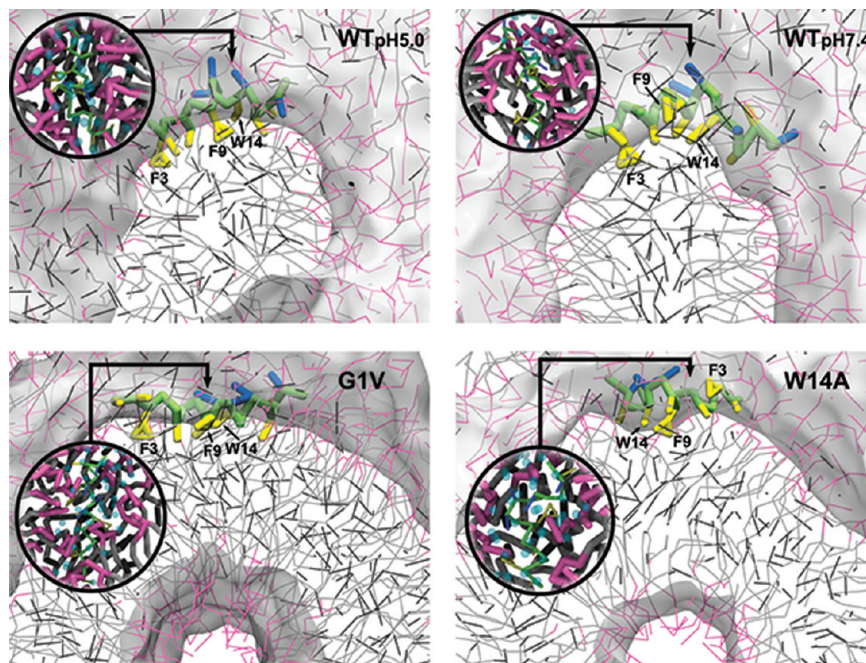


Figure 7. Positioning and embedding of the fusion peptides at the lipid/water interphase. Shown are the WT at pH 5.0 in the single diamond phase, and at pH 7.4 in the stalk phase. In addition, the G1V and W14A mutants are shown in the double diamond phase. The peptides locally replace the lipid headgroups and sit in a cradle-like lipid configuration. Lipid headgroups are shown in magenta, and tails are shown in gray (with black indicating the distal ends). The peptides' backbones are depicted in green, and hydrophilic and hydrophobic side chains in blue and yellow, respectively. In the main figure, the surface separating the lipid tails from the rest of the system has been rendered as transparent gray layer. Strongly hydrophobic amino acids with aromatic side chains have been labeled for better orientation. The inset shows a top view of the peptides' embedding; the viewpoint is indicated by the arrow.

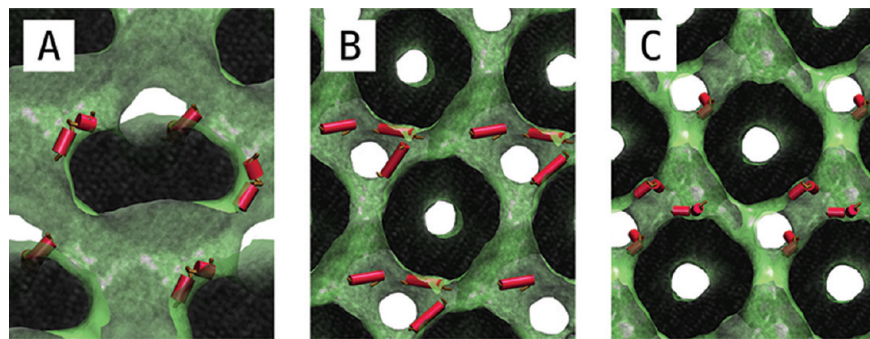


Figure 8. Images of the bicontinuous diamond phases illustrating the position of the influenza HA fusion peptides. Shown are the wild-type fusion peptides in a single diamond phase (A), and the G1V and W14A mutants in a double diamond phase (B and C). For all snapshots, the lipid composition is pure DOPE. The color representation is the same as in Figure 4 with red cylinders highlighting the peptides' helical parts.

and the Gaussian curvature gives the amount of saddle-splay deformation.

The two major changes of the phase diagram induced by the peptides (cf., Figure 3) are a change from the inverted hexagonal to the stalk phase for pure DOPE, and a change from the stalk phase toward the lamellar phase for pure DOPC and the 1:1 mixture. Both of these represent a shift toward positive mean curvature. An additional effect of the fusion peptides is the appearance of bicontinuous cubic phases, which, judging from our data for the wild-type peptides, is insensitive to the spontaneous mean curvature of the lipid mixture. These findings indicate a peptide-induced stabilization of Gaussian curvature. A reduction of the Gaussian curvature modulus as a result of peptide–lipid interplay has also been proposed by Siegel.³⁴

Given our ability to pinpoint the peptides' positions in the very anisotropic curvature landscapes of the nonlamellar phases, we do not need to limit our discussion to effects on the global curvature, as usually is the case using elastic theory.³³ This is especially important because packing and other membrane-perturbing effects in the vicinity of the peptides need to be taken into account, and membrane properties like spontaneous curvature and bending modulus can no longer be considered constant over the surface area.

By adsorbing to the lipid/water interface, peptides can modulate the preferred curvature in two ways, (i) via their contribution to the surface area and (ii) via their own shape. The first contribution is generic in the sense that any peptide adsorbed at the lipid/water interface will increase the effective volume of the headgroup region. In an additional series of simulations, we quantified this effect for isolated bilayers (see Supporting Information, Table 1). We found that symmetric insertion of the fusion peptides into a bilayer increases the surface area, suggesting a change toward more positive spontaneous mean curvature. The second effect is more specific and depends on the shape of the peptide and the corresponding influence on the accommodating surface. An anisotropic, elongated shape will enhance positive curvature stress in one principal direction. The WT peptide can promote positive curvature stress even to a higher degree via its pronounced boomerang shape. In combination with lipids with negative curvature, such as the unsaturated lipids in the current study, this mechanism allows for the stabilization of saddle splay curvature. In the WT-induced rhombohedral phase, the peptides are indeed found embracing the circular cross-section of the stalks (Figure 4B,C), lining up with the positive curvature component of the stalks. The colocalization is also nicely seen in the snapshots of the self-assembly process, with the peptides diffusing toward the stalks

once they have appeared (cf., Figure 2, snapshots at $t = 240$ ns and $12 \mu\text{s}$). The tendency to colocalize with the stalks is especially prominent for the pure DOPE system; in the mixture of DOPE/DOPC, the peptides are frequently found in the planar regions of the interface between the stalks (Figure 4E). In such a mixture, which also forms the rhombohedral phase in the absence of peptide, the peptide is not required to stabilize the curvature. In fact, the stalks present the regions with the most negative mean curvature, and the peptides shield away from it. In the cubic phases, the majority of the WT peptides is found to locate between two of the stalks emerging from the tetrahedral connections so that the helical arms are aligned with the positive component of the surface curvature (Figure 8A and Figure 7). While the induction of positive mean curvature by the fusion peptides appears to contradict experimental findings in which the peptides lower the lamellar-to-inverted hexagonal phase transition temperature,⁷ this may be due to a concentration dependence of the effects. At high concentration comparable to that in our simulations, the fusion peptides are found to increase the inverted hexagonal phase lattice constant in X-ray diffraction experiments,⁸ indicating a more positive mean curvature and supporting our interpretation.

The linear G1V mutant and the inverted W14A mutant, on the other hand, lack the wild-type's specific boomerang shape and can only induce an overall positive curvature via their contribution to the surface area. Consistent with this idea, the mutants are observed to disturb the phase diagram to a much lower degree as compared to the WT. Concerning the observed selectivity of the wild-type and mutant peptides in the stabilization of either the single or the double diamond phase, there is no difference in the total amount of Gaussian curvature per primitive unit cell between these two phases. However, the single diamond phase, which is only observed in the presence of the wild-type peptides, possesses the higher maximum positive principal curvature, in agreement with the wild-type's stronger ability to induce positive curvature via its shape contribution. The location of the mutant peptides in the double diamond phase is less clearly defined than that of the wild-type in the single diamond phase. While both mutants appear to locate preferably in the junctions of the network of water channels, a clear alignment with a positive or negative curvature component can neither be found for the G1V nor the W14A mutant. The linear G1V mutant appears to avoid orientations in which it would align with a large curvature component (Figure 8B and Figure 7), while the inverted kink of the W14A mutant often is found lying sideways on the lipid/water interface

rather than aligning with a negative curvature component (Figure 8C and Figure 7).

Similar to the mutants, the WT with the structure corresponding to pH 7.4 displays a reduced effectivity in promoting the stalk phase in the phase diagram of DOPE, showing a clear dependence on structure rather than sequence. Interestingly, the kink in the WT's backbone has a similar angle at both pH values. However, the distribution of the side chains is different. While the hydrophobic side chains are strongly aligned toward the inside of the kink at pH 5.0, this alignment is a lot less pronounced at pH 7.4 (Figure 7), presenting an explanation as to why at the latter pH the nonhelical C-terminal arm penetrates less deeply into the membrane. With the C-terminal arm lacking a strong preference to locate at the interface between the hydrophobic core and the headgroups, the WT's ability to distort the lipid/water interface via its boomerang shape can be expected to be reduced. In addition, a more shallow embedding reduces the peptides' general effect on curvature due to replacement of lipid headgroups.

The Role of the Fusion Peptide in Connection to Membrane Fusion. In light of the function of the HA fusion peptide *in vivo*, it is interesting to relate our findings to the potential role of these peptides in the fusion process. Traditionally, this role has been understood as the ability of fusion peptides to promote negative curvature. As such, the peptides are believed to facilitate the formation of stalks, which possess an overall negative curvature (e.g., refs 35,36). With stalks as the predicted initial step of the fusion pathway,³⁷ the link between the fusion peptide and membrane fusion is easily made. However, in contrast to this view, we observe local stabilization of positive curvature rather than negative curvature. On the molecular level, the fusion peptide appears to stabilize porous structures rather than stalks. Note that the stalk phase observed in our simulations for the mixture of the peptide with DOPE lipids is stable with respect to the inverted hexagonal phase and can be seen as a porated inverted hexagonal phase. In addition, one of the major differences we find between the WT and the nonfusogenic mutants appears to be the mutants' decreased ability to create pores, further suggesting an importance of porous structures in the fusion process.

To explicitly test the ability of the fusion peptides to promote stalk formation between lipid membranes, we performed an additional series of simulations in which the WT peptides were embedded between dehydrated lamellar samples (see the Supporting Information). Comparison of these simulations with simulations of peptide-free reference systems shows an inhibition of stalk formation in the presence of the peptides. This is consistent with our data obtained from the self-assembly simulations and indicates an increased energy of stalks in membranes for which the equilibrium phase in the absence of peptides is a lamellar configuration. Thus, our data do not support stabilization of the stalk as the mechanism by which the fusion peptides facilitate fusion.

It is therefore plausible that the fusion peptides act, at least partially, by facilitating a different stage of the fusion process. A potential candidate would be the stabilization of stalk–pore complexes that have been reported as intermediate stages in simulations investigating vesicle fusion.^{38–41} The morphology of the single diamond cubic phase corresponds to that of a periodic array of such stalk–pore complexes. Our simulations point to a stabilization of this phase in the presence of the wild-type fusion peptide. Occurrence of the stalk–pore complex during membrane fusion would explain the leaky fusion observed

experimentally during HA protein mediated membrane fusion.^{42,43} Interestingly, pores stabilized by fusion peptides have also been observed in recent coarse-grained simulations of SNARE-mediated fusion,⁴⁴ and in experimental studies on the fusogenic peptide from the parainfluenza virus S (PIVS).⁴⁵

The stabilization of double bicontinuous cubic phases is also considered an indicator of fusogenicity, due to the local resemblance of these phases to fusion pores. In that sense, our observation of the double diamond phase in the presence of the G1V and W14A mutants would indicate a facilitation of fusion in their presence, contrary to experimental findings. However, fusogenicity and stabilization of cubic phases are not always strictly related,⁴⁶ and at least for the fusion peptide of the simian immunodeficiency virus (SIV) a nonfusogenic mutant was found to stabilize these phases to a higher extent than the fusogenic wild-type.⁴⁷ In addition, our observation of the single instead of the double diamond phase in the presence of the wild-type peptides does not necessarily indicate that the wild-type cannot act to stabilize double bicontinuous cubic phases. Judging from our observation of the fusion peptides' general stabilization of negative Gaussian curvature, one would rather expect them to also decrease the energy of double phases and hence fusion pores, even though single phases might be stabilized even more due to their larger maximum positive curvature component, as argued above.

Finally, we hypothesize that the observed behavior for the HA fusion peptide can be used to explain data on membrane active peptides in general, providing a link between fusogenic peptides,^{35,48} antimicrobial peptides (AMPs),⁴⁹ and cell penetrating peptides.⁵⁰ An increasing amount of literature suggests that these traditional classifications are not rigid and some peptides may have multiple functionalities.^{51–57} Adsorbing at the interface, these peptides exert considerable stress on the monolayer to which they adsorb, which can be rationalized in terms of their wedge-like shape.⁵⁸ Poration is a way in which the excess stress can be relieved. In fact, it is generally viewed as the mode of action of antimicrobial peptides, causing cell content leakage or even complete lysis of the cell membrane. For isolated membranes, it is probably the only way, but under conditions where membranes are in close proximity (i.e., during fusion), the stalk–pore complex can form. In this respect, antimicrobial peptides may act similar to fusion peptides. Experimental work suggests that AMPs can also stabilize nonlamellar phases, and particularly inverted cubic phases.⁵⁹ Biophysical studies of the TAT protein transduction domain, a cell-penetrating peptide, also reveal stabilization of inverted cubic phases.⁶⁰ The ability of AMPs to induce saddle-splay curvature has furthermore been linked to the lipid composition of the membrane and has been implicated to be a generic mechanism for membrane remodeling.⁶¹

■ METHODS

System Details. The systems simulated consist of 256 molecules of lipid (either pure DOPE, DOPC, or a 1:1 mixture), 4 or no fusion peptides, and between 2 and 3 coarse-grained water beads per lipid (representing actual hydration levels of 8–12 water molecules per lipid and including sodium ions to counter the charges of the peptides). The initial system consisted of a random mixture of these components in a cubic box, obtained from a short NVT relaxation run in which all nonbonded interactions in the system were set to be similar to those between water beads. Subsequent self-assembly simulations were performed in an NPT ensemble over a total of 75×10^6 steps, corresponding to an effective simulation time of 12 μ s. This time proved to be sufficient for the system to adopt a (kinetically) stable

state with no phase changes during the last 4 μ s of the simulation. Multiple simulations starting from different initial velocities were run for each system and set of conditions. Some additional self-assembly simulations were performed for 8-times bigger systems. Unfortunately, these systems showed a high tendency to become kinetically trapped in irregular structures and were not further considered. Test systems constructed from periodically replicating some of the final configurations obtained with our standard systems, however, always remained stable with no signs of phase changes. An example can be found in the Supporting Information of ref 24.

Simulation Parameters. The simulations shown were performed using the coarse-grained MARTINI model, version 2.1^{19,20} with the Gromacs-3.3 software package⁶² using the standard run-parameters for the MARTINI model at a time step of 40 fs. Both pressure and temperature were coupled to a reference value using the Berendsen scheme.⁶³ The self-assembly simulations were carried out with anisotropic pressure coupling with a compressibility of 5×10^{-5} bar⁻¹ for the diagonal elements and 1×10^{-7} bar⁻¹ for the off-diagonal elements of the pressure tensor, coupling time constants of 1.2 ps, and reference pressures of 1.0 bar. The reference temperatures were set to values ranging from 270 to 315 K with a coupling time constant of 0.5 ps. Lennard-Jones and Coulomb interactions were obtained every step for particles within a cutoff of 1.2 nm according to a neighbor list updated every 10 steps. Both the Lennard-Jones and the Coulomb potential were modified with a shift function to have the interactions smoothly vanishing at the cutoff. Electrostatic interactions were screened with an effective dielectric constant of 15.

Models for the Fusion Peptides. The models for the fusion peptides were based on NMR structures obtained in micelles.^{5,9,11} Particle types and bonded interactions were set according to the standard MARTINI protocol. Note that the secondary structure is preassigned in the model, based on the NMR data, constraining the angles and dihedral angles in the peptide backbone to match the experimental structure. A comparison of our peptide models and the experimental structures is given in Figure 1. Details and further alterations for the individual peptides are given in the Supporting Information.

Phase Determination. Phases were characterized by their topology, that is, the connectivity of the hydrophobic and the hydrophilic regions, which does not depend on the exact shape and is insensitive to mere deformations like stretching or bending. Specifically, we looked at the topology of the volume occupied by the water beads and lipid headgroups and assigned the phase for which the topology matches. This approach is unambiguous and in addition directly related to the structural elements, for example, stalks and pores, which are at the heart of the topic under discussion. A description of the use of morphological features in phase determination can be found in a recent work by the authors.⁶⁴

ASSOCIATED CONTENT

Supporting Information

Details about the parametrization of the influenza HA fusion peptide and its G1V and W14A mutant, a detailed version of the phase diagram shown in Figure 3 indicating the exact temperature and level of solvation, and additional simulations of the peptides' effect on stalk formation in lamellar systems at low hydration. This material is available free of charge via the Internet at <http://pubs.acs.org>.

AUTHOR INFORMATION

Corresponding Author

s.j.marrink@rug.nl

ACKNOWLEDGMENTS

Support from The Netherlands Organization for Scientific Research (NWO) is thankfully acknowledged.

REFERENCES

- (1) Cross, K. J.; Langley, W. A.; Russell, R. J.; Skehel, J. J.; Steinhauer, D. A. *Protein Pept. Lett.* **2009**, *16*, 766–778.
- (2) Armstrong, R. T.; Kushnir, A. S.; White, J. M. *J. Cell Biol.* **2000**, *151*, 425–437.
- (3) Steinhauer, D. A.; Wharton, S. A.; Skehel, J. J.; Wiley, D. C. *J. Virol.* **1995**, *69*, 6643–6651.
- (4) Carr, C. M.; Chaudhry, C.; Kim, P. S. *Proc. Natl. Acad. Sci. U.S.A.* **1997**, *94*, 14306–14313.
- (5) Lai, A. L.; Park, H.; White, J. M.; Tamm, L. K. *J. Biol. Chem.* **2006**, *281*, 5760–5770.
- (6) Han, X.; Tamm, L. K. *Proc. Natl. Acad. Sci. U.S.A.* **2000**, *97*, 13097–13102.
- (7) Epand, R. M.; Epand, R. F. *Biochem. Biophys. Res. Commun.* **1994**, *202*, 1420–1425.
- (8) Siegel, D. P.; Epand, R. M. *Biochim. Biophys. Acta, Biomembr.* **2000**, *1468*, 87–98.
- (9) Han, X.; Bushweller, J. H.; Cafiso, D. S.; Tamm, L. K. *Nat. Struct. Biol.* **2001**, *8*, 715–720.
- (10) Lorieau, J. L.; Louis, J. M.; Bax, A. *Proc. Natl. Acad. Sci. U.S.A.* **2010**, *107*, 11341–11346.
- (11) Li, Y.; Han, X.; Lai, A. L.; Bushweller, J. H.; Cafiso, D. S.; Tamm, L. K. *J. Virol.* **2005**, *79*, 12065–12076.
- (12) Marrink, S. J.; de Vries, A. H.; Tieleman, D. P. *Biochim. Biophys. Acta, Biomembr.* **2009**, *1788*, 149–168.
- (13) Lindahl, E.; Sansom, M. S. P. *Curr. Opin. Struct. Biol.* **2008**, *18*, 425–431.
- (14) Gurtovenko, A. A.; Anwar, J.; Vattulainen, I. *Chem. Rev.* **2010**, *110*, 6077–6103.
- (15) Ayton, G. S.; Blood, P. D.; Voth, G. A. *Biophys. J.* **2007**, *92*, 3595–3602.
- (16) Huang, Q.; Chen, C. L.; Herrmann, A. *Biophys. J.* **2004**, *87*, 14–22.
- (17) Li, J.; Das, P.; Zhou, R. *J. Phys. Chem. B* **2010**, *114*, 8799–8806.
- (18) Lagüe, P.; Roux, B.; Pastor, R. W. *J. Mol. Biol.* **2005**, *354*, 1129–1141.
- (19) Marrink, S. J.; Risselada, H. J.; Yefimov, S.; Tieleman, D. P.; de Vries, A. H. *J. Phys. Chem. B* **2007**, *111*, 7812–7824.
- (20) Monticelli, L.; Kandasamy, S. K.; Periole, X.; Larson, R. G.; Tieleman, D. P.; Marrink, S. J. *J. Chem. Theory Comput.* **2008**, *4*, 819–834.
- (21) Marrink, S. J.; Mark, A. E. *Biophys. J.* **2004**, *87*, 3894–3900.
- (22) Risselada, H. J.; Marrink, S. J. *Proc. Natl. Acad. Sci. U.S.A.* **2008**, *105*, 17367–17372.
- (23) Kučerka, N.; Marquardt, D.; Harroun, T. A.; Nieh, M. P.; Wassall, S. R.; de Jong, D. H.; Schäfer, L. V.; Marrink, S. J.; Katsaras, J. *Biochemistry* **2010**, *49*, 7485–7493.
- (24) Fuhrmans, M.; Knecht, V.; Marrink, S. J. *J. Am. Chem. Soc.* **2009**, *131*, 9166–9167.
- (25) Rzepiela, A. J.; Sengupta, D.; Goga, N.; Marrink, S. J. *Faraday Discuss.* **2009**, *144*, 431–443.
- (26) Schäfer, L. V.; de Jong, D. H.; Holt, A.; Rzepiela, A. J.; de Vries, A. H.; Poolman, B.; Killian, J. A.; Marrink, S. J. *Proc. Natl. Acad. Sci. U.S.A.* **2011**, *108*, 1343–1348.
- (27) Chernomordik, L. V.; Kozlov, M. M. *Nat. Struct. Mol. Biol.* **2008**, *15*, 675–683.
- (28) Rand, R. P.; Fuller, N. L. *Biophys. J.* **1994**, *66*, 2127–2138.
- (29) Yang, L.; Ding, L.; Huang, H. W. *Biochemistry* **2003**, *42*, 6631–6635.
- (30) Marrink, S. J.; Mark, A. E. *J. Am. Chem. Soc.* **2003**, *125*, 15233–15242.
- (31) Gandy, P. J. F.; Cvijovic, D.; Mackay, A. L.; Klinowski, J. *Chem. Phys. Lett.* **1999**, *314*, 543–551.
- (32) Katsov, K.; Müller, M.; Schick, M. *Biophys. J.* **2006**, *90*, 915–926.
- (33) Hyde, S.; Andersson, S.; Larsson, K.; Blum, Z.; Landh, T.; Lidin, S.; Ninham, B. W. *The Language of Shape*; Elsevier: New York, 1997.
- (34) Siegel, D. P. The relationship between bicontinuous inverted cubic phases and membrane fusion. In *Bicontinuous Liquid Crystals*;

- Lynch, M. L.; Spicer, P. T., Eds.; Taylor and Francis: New York, 2005; pp 59–98.
- (35) Epand, R. M. *Biochim. Biophys. Acta, Biomembr.* **2003**, *1614*, 116–121.
- (36) Zemel, A.; Ben-Shaul, A.; May, S. *J. Phys. Chem. B* **2008**, *112*, 6988–6996.
- (37) Kozlovsky, Y.; Chernomordik, L. V.; Kozlov, M. M. *Biophys. J.* **2002**, *83*, 2634–2651.
- (38) Noguchi, H.; Takasu, M. *J. Chem. Phys.* **2001**, *115*, 9547–9551.
- (39) Marrink, S. J.; Fuhrmans, M.; Risselada, H. J.; Periole, X. The MARTINI Forcefield. In *Coarse-Graining of Condensed Phase and Biomolecular Systems*; Voth, G., Ed.; CRC Press: New York, 2008.
- (40) Markvoort, A. J.; Marrink, S. J. *Curr. Top. Membr.* **2011**, *68*, 259–294.
- (41) Müller, M.; Katsov, K.; Schick, M. *J. Chem. Phys.* **2002**, *116*, 2342–2345.
- (42) Frolov, V. A.; Dunina-Barkovskaya, A. Y.; Samsonov, A. V.; Zimmerberg, J. *Biophys. J.* **2003**, *85*, 1725–1733.
- (43) Haque, M. E.; Chakraborty, H.; Koklic, T.; Komatsu, H.; Axelsen, P. H.; Lentz, B. R. *Biophys. J.* **2011**, *101*, 1095–1104.
- (44) Risselada, H. J.; Kutzner, C.; Grubmüller, H. *ChemBioChem* **2011**, *12*, 1049–1055.
- (45) Donald, J. E.; Zhang, Y.; Fiorin, G.; Carnevale, V.; Slochower, D. R.; Gai, F.; Klein, M. L.; DeGrado, W. F. *Proc. Natl. Acad. Sci. U.S.A.* **2011**, *108*, 3958–3963.
- (46) Epand, R. M.; Epand, R. F.; Martin, I.; Ruysschaerts, J. M. *Biochemistry* **2001**, *40*, 8800–8807.
- (47) Colotto, A.; Martin, I.; Ruysschaert, J. M.; Sen, A.; Hui, S. W.; Epand, R. M. *Biochemistry* **1996**, *35*, 980–989.
- (48) Tamm, L. K.; Han, X.; Li, Y.; Lai, A. L. *Pept. Sci.* **2002**, *66*, 249–260.
- (49) Brogden, K. A. *Nat. Rev. Microbiol.* **2005**, *3*, 238–250.
- (50) Järver, P.; Langel, U. *Biochim. Biophys. Acta* **2006**, *1758*, 260–263.
- (51) Lai, A. L.; Tamm, L. K. *J. Biol. Chem.* **2010**, *285*, 37467–37475.
- (52) Yang, S. T.; Zaitseva, E.; Chernomordik, L. V.; Melikov, K. *Biophys. J.* **2010**, *99*, 2525–2533.
- (53) Nicolas, P. *FEBS J.* **2009**, *276*, 6483–6496.
- (54) Almeida, P. F.; Pokorný, A. *Biochemistry* **2009**, *48*, 8083–8093.
- (55) Hale, J. D. F.; Hancock, R. E. W. *Expert Rev. Anti-Infect. Ther.* **2007**, *5*, 951–959.
- (56) Wadhwani, P.; Reichert, J.; Bürck, J.; Ulrich, A. S. *Eur. Biophys. J.* **2011**, DOI: 10.1007/s00249-011-0771-7.
- (57) Cirac, A. D.; Moiset, G.; Mika, J. T.; Koçer, A.; Salvador, P.; Poolman, B.; Marrink, S. J.; Sengupta, D. *Biophys. J.* **2011**, *100*, 2422–2431.
- (58) Bechinger, B. *Curr. Opin. Colloid Interface Sci.* **2009**, *14*, 349–355.
- (59) Haney, E. F.; Nathoo, S.; Vogel, H. J.; Prenner, E. J. *J. Chem. Phys. Lipids* **2010**, *163*, 82–93.
- (60) Mishra, A.; Gordon, V. D.; Yang, L.; Coridan, R.; Wong, G. C. L. *Angew. Chem., Int. Ed.* **2008**, *47*, 2986–2989.
- (61) Schmidt, N. W.; Mishra, A.; Lai, G. H.; Davis, M.; Sanders, L. K.; Tran, D.; Garcia, A.; Tai, K. P.; McCray, P. B.; Ouellette, A. J.; Selsted, M. E.; Wong, G. C. *J. Am. Chem. Soc.* **2011**, *133*, 6720–6727.
- (62) van der Spoel, D.; Lindahl, E.; Hess, B.; Groenhof, G.; Mark, A. E.; Berendsen, H. J. C. *J. Comput. Chem.* **2005**, *26*, 1701–1718.
- (63) Berendsen, H. J. C.; Postma, J. P. M.; DiNola, A.; Haak, J. R. *J. Chem. Phys.* **1984**, *81*, 3684–3690.
- (64) Fuhrmans, M.; Marrink, S. J. *J. Mol. Model.* **2011**, *17*, 1755–1766.